Keggin-type polyoxometalate 1:1 complexes of Pb(II) and Bi(III): experimental, theoretical and luminescence studies

Anna A. Mukhacheva,[a] Tatiana Asanova,[a] Maxim R. Ryzhikov,[a] Taisiya S. Sukhikh,[a] Nikolay B. Kompankov,[a] Vadim V. Yanshole,[b,c] Alexey S. Berezin,[a] Artem L. Gushchin,[a] Pavel A. Abramov,*[a,d] Maxim N. Sokolov [a]

a Nikolayev Institute of Inorganic Chemistry, 3 Akad. Lavrentiev Ave. 630090, Russia;

b International Tomography Center, Institutskaya str. 3a, 630090, Novosibirsk, Russia;

c Novosibirsk State University, Pirogova str. 1, 630090, Novosibirsk, Russia;

d South Ural State University, Prospekt Lenina, 76, 454080, Chelyabinsk, Russia;

Supporting information

Table of contents

Experimental part

General information

$K_7[PW_{11}O_{39}]\cdot 14H_2O$ was synthesized according to the literature.[1] Other reagents were of commercial quality and were used as purchased. Elemental analysis was carried out on a Eurovector EA 3000 CHN analyzer. Energy-dispersive X-ray spectroscopy (EDS) was performed on a Hitachi TM3000 TableTop SEM with Bruker QUANTAX 70 EDS equipment.

NMR

^{183}W and ^{31}P NMR spectra were recorded on a Bruker Avance III 500 spectrometer using internal standards.

HR-ESI-MS

The high-resolution electrospray ionization mass spectrometric (HR-ESI-MS) measurements were performed at the Center of Collective Use «Mass spectrometric investigations» SB RAS. Spectra were obtained with a direct injection of liquid samples on an ESI quadrupole time-of-flight (ESI-q-TOF) high-resolution mass spectrometer Maxis 4G (Bruker Daltonics, Germany). The spectra were recorded in the 300-3000 m/z range in negative mode.

Calculations

Quantum-chemical calculations was performed in ADF2013 program suite with VWN+BP86 density functional and TZP (core double-ζ, valence triple-ζ, polarized) basis set (ADF2013, SCM, Theoretical Chemistry, Vrije Universiteit, Amsterdam, The Netherlands, http://www.scm.com).[2–5] Full geometry optimization was performed with quasi Newton approach.[6] The ZORA[12] approximation was used to take into account scalar relativistic effects. The spin restricted approximation was used for all calculations. The absences of imaginary frequencies confirming that the all calculated complexes are in local energy minima. The similar theoretical level was used earlier for the calculations of the tungsten POMs.[7,8] The ELF (Electron Localization Function) distribution and QTAIM (Quantum Theory of Atoms In Molecules) critical points location was calculated in dgrid-4.6 program (M. Kohout, DGrid, version 4.6, Radebeul, 2011).[9,10] The QTAIM atomic charges calculated in ADF2013 program suite.

In order to identify experimental NMR chemical shifts for ^{183}W, the shielding constants were calculated by DFT method in ADF2019 program suit. The geometry optimization of $[PW_{11}O_{39}Bi]^{4-}$ and $[PW_{11}O_{39}Pb]^{5-}$ complexes was performed with PBE0 [11,12] density functional, Grimme D4(EEQ) dispersion corrections [13], all-electron TZP basis set, scalar relativistic approximation ZORA[14] and COSMO[15] method to simulate DMF environment. Since the inclusion of the spin-orbit coupling improve the calculated NMR data[7,8], the tungsten shielding constants were calculated for optimized structures within spin-orbit relativistic ZORA[16]

approximation by GIAO[17] method while the rest of the theoretical level was the same as for geometry optimization.

Electrochemistry

The cyclic voltammograms (CV) were recorded with a 797 VA Computrace system (Metrohm, Switzerland). All measurements were performed with a conventional three-electrode configuration consisting of glassy carbon working and platinum auxiliary electrodes and an Ag/AgCl/KCl reference electrode. The solvent used in all experiments was CH_3CN which was deoxygenated before use. Tetra-n-butylammonium hexafluorophosphate (0.1 M solution) was used as a supporting electrolyte. The concentration of the complexes was approximately 10^{-3} M. Redox potential values ($E_{1/2}$) were determined as $(E_a + E_c)/2$, where E_a and E_c are anodic and cathodic peak potentials, respectively. Ferrocene was used as an internal standard, the Fc/Fc+ potential was 0.43 V.

EXAFS

EXAFS spectra of **1**, **2**, **2-ox** and reference compounds PbO, PbO_2 were measured at 10C beamline of PLSII (Pohang Accelerator Laboratory, South Korea). The ring current was 400 mA at 3.0 GeV. A Si(111) double crystal monochromator was used.

The IFEFFIT software package[18] was employed for EXAFS spectra interpretation. Quantitative EXAFS-parameters were determined using a fitting procedure with the following parameters: wave number (k) and interatomic distance (r) ranges were 2.7-10.0Å^{-1} and 1.1-4.0Å, respectively, EXAFS-function was k^2-weighted. As an initial structural model was used PbO with tetragonal space grope *P*4/nmm. In the fitting procedure, the spectroscopic factor S_0^2 was determined to be 0.81(3) for PbO, and then the value was fixed for the studied samples.

Synthesis of $(Bu_4N)_4[PW_{11}O_{39}Bi]$ (1):

3.3 g (1 mmol) $K_7[PW_{11}O_{39}]\cdot 14H_2O$ was dissolved upon heating in 15 mL of 4M acetate buffer (pH=5.0) **(a)**. $Bi(NO_3)_3\cdot 5H_2O$ (0.5 g, 1 mmol) was dissolved upon heating in concentrated nitric acid (1.5 mL) **(b)**. After cooling to room temperature solution **(b)** was added dropwise to **(a)** avoiding precipitation. The solutions were stirred during 0.5 h and then $(Bu_4N)Br$ was added to full precipitation. The solution was filtered on a glass filter and precipitate was washed with a large amount of distilled water. Yield 3.5 g (87% based on $K_7PW_{11}O_{39}\cdot 14H_2O$). IR (ATR, cm^{-1}): 1482 (m), 1380 (w), 1084 (m), 1052 (m), 951 (s), 880 (m), 789 (vs), 594 (m). EDX found: 50% W, 5.4% Bi, 0.7% P; calc for **1**: 51.8% W, 5.4% Bi, 0.8% P. C, H, N found (%): 20.5; 3.8; 1.5; calculated for 1 C, H, N (%): 20.0; 3.8; 1.4. ^{31}P NMR (CD_3CN, r.t., δ): -11.3 ppm; ^{183}W NMR (DMF/CD_3CN, r.t., δ): -53.4, -91.2, -94.9, -97.6, -118.7, -122.3 ppm. HR-ESI-MS(-): m/z

721.550 $[BiPW_{11}O_{39}]^{4-}$; m/z 962.398 $\{HBiPW_{11}O_{39}\}^{3-}$; m/z 1042.883 $\{(Bu_4N)BiPW_{11}O_{39}\}^{3-}$; m/z 1564.830 $\{(Bu_4N)HBiPW_{11}O_{39}\}^{2-}$; m/z 1685.558 $\{(Bu_4N)_2BiPW_{11}O_{39}\}^{2-}$.

Synthesis of $(Bu_4N)_5[PW_{11}O_{39}Pb]$ (2):

3.5 g (1.6 mmol) of $K_7PW_{11}O_{39}\cdot 14H_2O$ was dissolved upon heating in 20 mL of 4M acetate buffer (pH=5.0). Solution of $Pb(NO_3)_2$ (1.6 mmol, 0.517 g in 2 mL H_2O) was added dropwise to cooled solution of the lacunary POM. After 0.5 h of stirring $(Bu_4N)Br$ was added to full precipitation. The solution was filtered on a glass filter and precipitate was washed with large amount of water. Resulted product was dissolved in a minimal amount of DMF, precipitated by addition of the diethyl ether and cooled in a refrigerator for aggregation. Then organic layer was removed and the precipitate was dried in a desiccator during several days. Yield 4.3 g (65% based on $K_7PW_{11}O_{39}\cdot 14H_2O$). IR (ATR, cm^{-1}) 1664 (w), 1482 (m), 1381 (w), 1083 (m), 1040 (m), 941 (s), 875 (s), 790 (vs), 672 (s), 590 (m). EDX found: 47% W, 5.1% Pb, 0.7% P; calculated for **2**: 48% W, 4.9% Pb, 0.7% P. C, H, N found (%): 22.4, 4.2, 1.8; calculated for **2** C, H, N (%): 22.7, 4.6, 1.7. ^{31}P NMR (CD_3CN, r.t., δ): -10.6 ppm; ^{183}W NMR (DMF/CD_3CN, r.t., δ): -51.9, -78.4, -96.4, -101.6, -118.8, -133.6 ppm. HR-ESI-MS(-): m/z 1042.630 $\{(Bu_4N)HPbPW_{11}O_{39}\}^{3-}$; m/z 1123.118 $\{(Bu_4N)_2PbPW_{11}O_{39}\}^{3-}$; m/z 1685.179 $\{(Bu_4N)_2HPbPW_{11}O_{39}\}^{2-}$; m/z 1805.911 $\{(Bu_4N)_3PbPW_{11}O_{39}\}^{2-}$.

Synthesis of $((CH_3)_4N)_4K_3[H_4(PW_{11}O_{39})_2Bi]\cdot 25H_2O$ (3):

$K_7[PW_{11}O_{39}]\cdot 14H_2O$ (2.170 g, 0.68 mmol) and $BiBr_3$ (0.152 g, 0.34 mmol) were dissolved in bi-distilled water (15 mL) and stirred at room temperature for 24 h. The precipitated white solid was removed by filtration and $(CH_3)_4NBr$ (0.1 g) was added according to the Sadakane's procedure.[19] While the initial pH was 5.65 and then it was adjusted to 3.95 by 3M HNO_3. After 1 week in a refrigerator crystals did not form, so we added more $(CH_3)_4NBr$ (0.7 g) and placed the crystallization dish into a refrigerator (5 °C) for 24 h. This leads to a crop of colorless block crystals of **3** instead of $(CH_3)_4N)_8(NH_4)_3[(PW_{11}O_{39})_2Bi]\cdot 55H_2O\cdot 0.3KCl\cdot 1(CH_3)_4NCl$. Yield of **3**: 1.4 g (64% by POM). EA: found C, H, N (%): 3.1, 1.5, 0.8; calc C,H,N (%): 3.0, 1.6, 0.9. ICP-AES: found K, P, Bi, W (%): 1.7, 0.7, 3.3, 63.0; calc K, P, Bi, W (%): 1.8, 0.9, 3.2, 62.9. IR (ATR, cm^{-1}): 1619(m), 1482(m), 1449(w), 1416(w), 1091(m), 1040(m), 941(s), 881(m), 858(m), 800(s), 753(vs), 661(vs), 583(vs).

References:

(1) Contant, R.; Thouvenot, R. Hétéropolyanions de Type Dawson. 2. Synthèses de Polyoxotungstoarsénates Lacunaires Dérivant de l'octadécatungstodiarsénate. Étude Structurale Par RMN Du Tungstène-183 Des Octadéca(Molybdotungstovanado)Diarsénates Apparentés. *Can. J. Chem.* **1991**, *69* (10), 1498–1506.

(2) Vosko, S. H.; Wilk, L.; Nusair, M. Accurate Spin-Dependent Electron Liquid Correlation Energies for Local Spin Density Calculations: A Critical Analysis. *Can. J. Phys.* **1980**, *58* (8), 1200–1211.

(3) Becke, A. D. Density-Functional Exchange-Energy Approximation with Correct Asymptotic Behavior. *Phys. Rev. A* **1988**, *38* (6), 3098–3100.

(4) Perdew, J. P. Density-Functional Approximation for the Correlation Energy of the Inhomogeneous Electron Gas. *Phys. Rev. B* **1986**, *33* (12), 8822–8824.

(5) Van Lenthe, E.; Baerends, E. J. Optimized Slater-Type Basis Sets for the Elements 1-118. *J. Comput. Chem.* **2003**, *24* (9), 1142–1156.

(6) Versluis, L.; Ziegler, T. The Determination of Molecular Structures by Density Functional Theory. The Evaluation of Analytical Energy Gradients by Numerical Integration. *J. Chem. Phys.* **1988**, *88* (1), 322–328.

(7) Vankova, N.; Heine, T.; Kortz, U. NMR Chemical Shifts of Metal Centres in Polyoxometalates: Relativistic DFT Predictions. *Eur. J. Inorg. Chem.* **2009**, *2009* (34), 5102–5108.

(8) Rodriguez-Fortea, A.; Alemany, P.; Ziegler, T. Density Functional Calculations of NMR Chemical Shifts with the Inclusion of Spin−Orbit Coupling in Tungsten and Lead Compounds. *J. Phys. Chem. A* **1999**, *103* (41), 8288–8294.

(9) Bader, R. F. W. *Atoms in Molecules : A Quantum Theory*; Clarendon Press, 1990.

(10) Silvi, B.; Savin, A. Classification of Chemical Bonds Based on Topological Analysis of Electron Localization Functions. *Nature* **1994**, *371* (6499), 683–686.

(11) Grimme, S. Accurate Description of van Der Waals Complexes by Density Functional Theory Including Empirical Corrections. *J. Comput. Chem.* **2004**, *25* (12), 1463–1473.

(12) Ernzerhof, M.; Scuseria, G. E. Assessment of the Perdew–Burke–Ernzerhof Exchange-Correlation Functional. *J. Chem. Phys.* **1999**, *110* (11), 5029–5036.

(13) Caldeweyher, E.; Ehlert, S.; Hansen, A.; Neugebauer, H.; Spicher, S.; Bannwarth, C.; Grimme, S. A Generally Applicable Atomic-Charge Dependent London Dispersion Correction. *J. Chem. Phys.* **2019**, *150* (15), 154122.

(14) van Lenthe, E.; Ehlers, A.; Baerends, E.-J. Geometry Optimizations in the Zero Order Regular Approximation for Relativistic Effects. *J. Chem. Phys.* **1999**, *110* (18), 8943–8953.

(15) Pye, C. C.; Ziegler, T. An Implementation of the Conductor-like Screening Model of Solvation within the Amsterdam Density Functional Package. *Theor. Chem. Accounts Theory, Comput. Model. (Theoretica Chim. Acta)* **1999**, *101* (6), 396–408.

(16) van Lenthe, E.; Snijders, J. G.; Baerends, E. J. The Zero-order Regular Approximation for Relativistic Effects: The Effect of Spin–Orbit Coupling in Closed Shell Molecules. *J. Chem. Phys.* **1996**, *105* (15), 6505–6516.

(17) Wolff, S. K.; Ziegler, T. Calculation of DFT-GIAO NMR Shifts with the Inclusion of Spin-Orbit Coupling. *J. Chem. Phys.* **1998**, *109* (3), 895–905.

(18) Ravel, B.; Newville, M. ATHENA , ARTEMIS , HEPHAESTUS : Data Analysis for X-Ray Absorption Spectroscopy Using IFEFFIT. *J. Synchrotron Radiat.* **2005**, *12* (4), 537–541.

Table S1. ^{31}P and ^{183}W NMR data for $[PW_{11}O_{39}Bi]^{4-}$, $[(PW_{11}O_{39})_2Bi]^{11-}$ and $[PW_{11}O_{39}Pb]^{5-}$ polyanions.

Anion	^{31}P (ppm)	^{183}W ppm (conditions)	Ref
$[PW_{11}O_{39}Bi]^{4-}$	-11.3	-53.4, -91.2, -94.9, -97.6, -118.7, -122.3; (DMF/CD_3CN mixture (80:20) at room temperature)	This work
	-11.5	-77.54, -98.37, -108.18, -108.33, -129.01, -140.04 (D_2O, room temperature)	Sadakane[19]
	-12.5	-40.61, -60.35, -92.49, -102.31, -115.70, -121.22 (CD_3CN, room temperature)	Izuage[20]
		-78.8, -100.2, -109.5, -130.1, -140.9 (D_2O, room temperature)	Maksimov[21]
$[(PW_{11}O_{39})_2Bi]^{11-}$		-94.5 (wide), -106.3, -114.5, -130.2, -150.7 (D_2O, room temperature)	Maksimov[21]
	-11.4	-104.49, -110.83, -147.98, -85.68, -93.86, -125.66 (D_2O, room temperature)	Sadakane[19]
$[PW_{11}O_{39}Pb]^{5-}$	-10.6	-51.9, -78.4, -96.4, -101.6, -118.8, -133.6 (DMF/CD_3CN mixture (80:20) at room temperature)	This work
	-11.9	-48.92, -77.53, -92.57, -97.77, -116.18, -129.90 (CD_3CN, room temperature)	Izuage[20]
		-78.7, -85.8, -106.0, -113.6, -129.8, -150.1 (D_2O, pH 2)	Maksimov[22]

(19) Wihadi, M. N. K.; Hayashi, A.; Ichihashi, K.; Ota, H.; Nishihara, S.; Inoue, K.; Tsunoji, N.; Sano, T.; Sadakane, M. A Sandwich Complex of Bismuth Cation and Mono-Lacunary α-Keggin-Type Phosphotungstate: Preparation and Structural Characterisation. *Eur. J. Inorg. Chem.* **2019**, *2019* (3–4), 357–362.

(20) Izuagie, T. Synthesis of Polyoxometalates ForDetailed Solution Reactivity Studies, Newcastle University, 2017.

(21) Maksimov, G. M. Maksimovskaya, R. I. Kozhevnikov, I. V. Heteropoly Acids Derived from the Complexes of the PW11O397−anion with Metal Cations. *Russ. J. Inorg. Chem.* **1992**, *37*, 2279–2286.

(22) Fedotov, M. A.; Maksimovskaya, R. I.; Maksimov, G. M.; Matveev, K. I. No Title. *Zh. Neorg. Khimii* **1987**, *32*, 647–651.

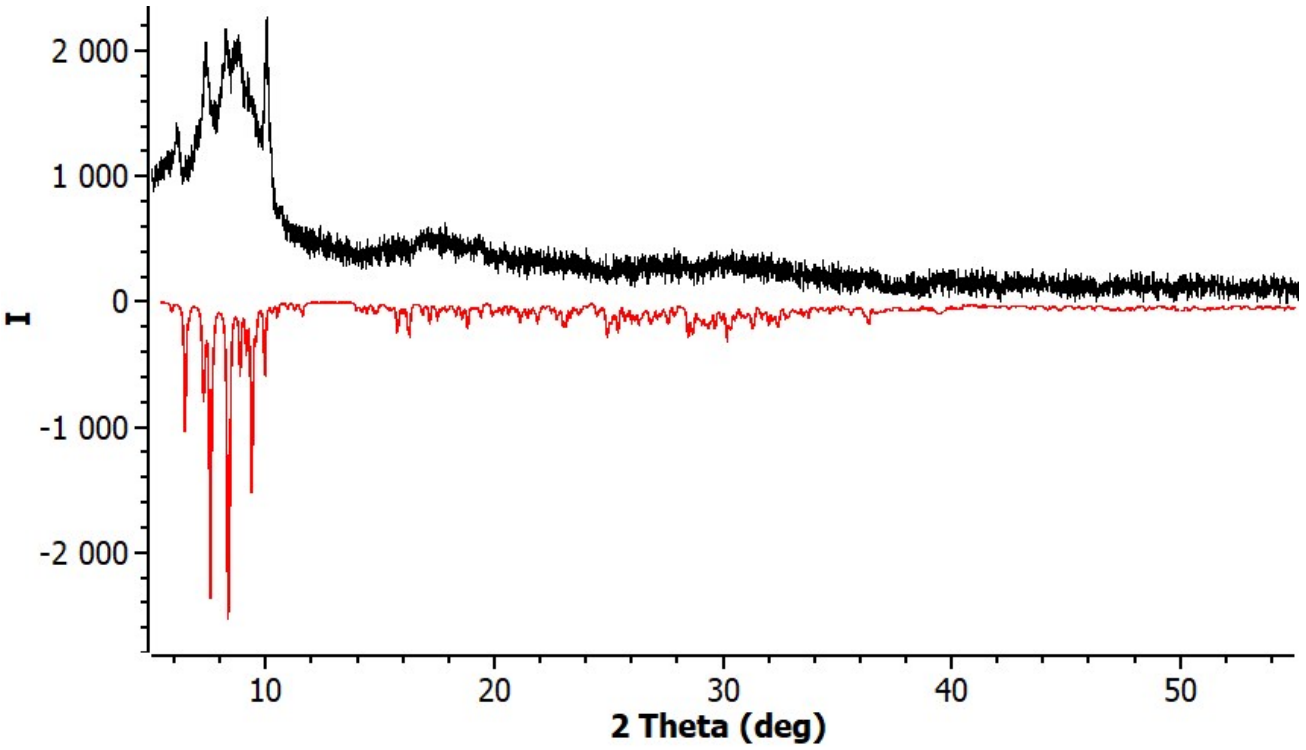

Fig. S1. XRPD data for **3**.

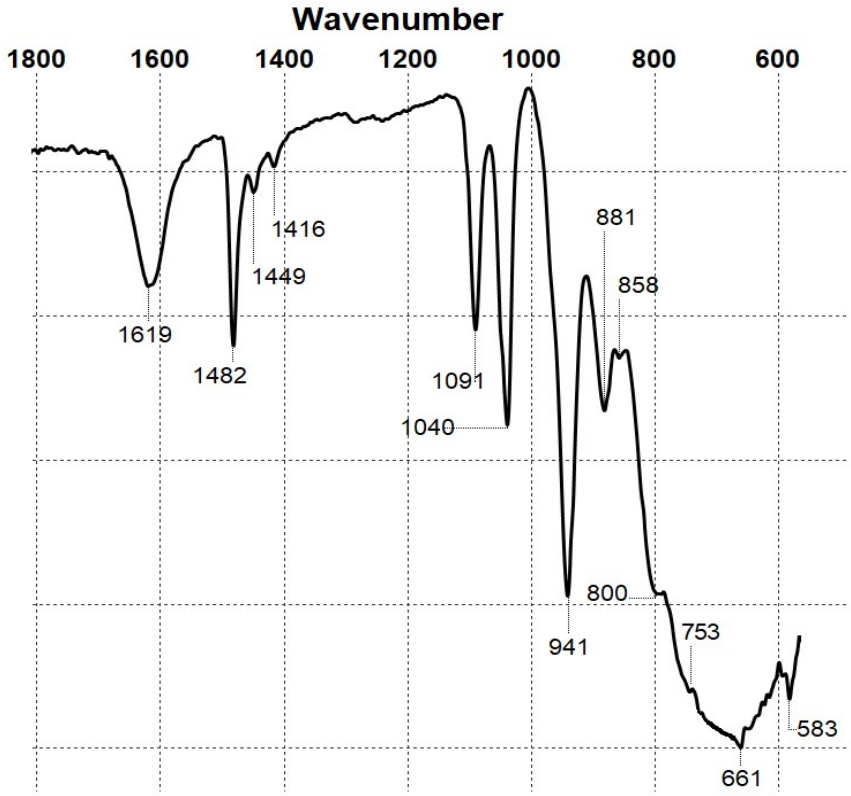

Fig. S2. IR spectrum of **3**.

HR-ESI-MS data

Fig. S3. Full HR-ESI-MS(-) spectrum of **1** in CH_3CN solution.

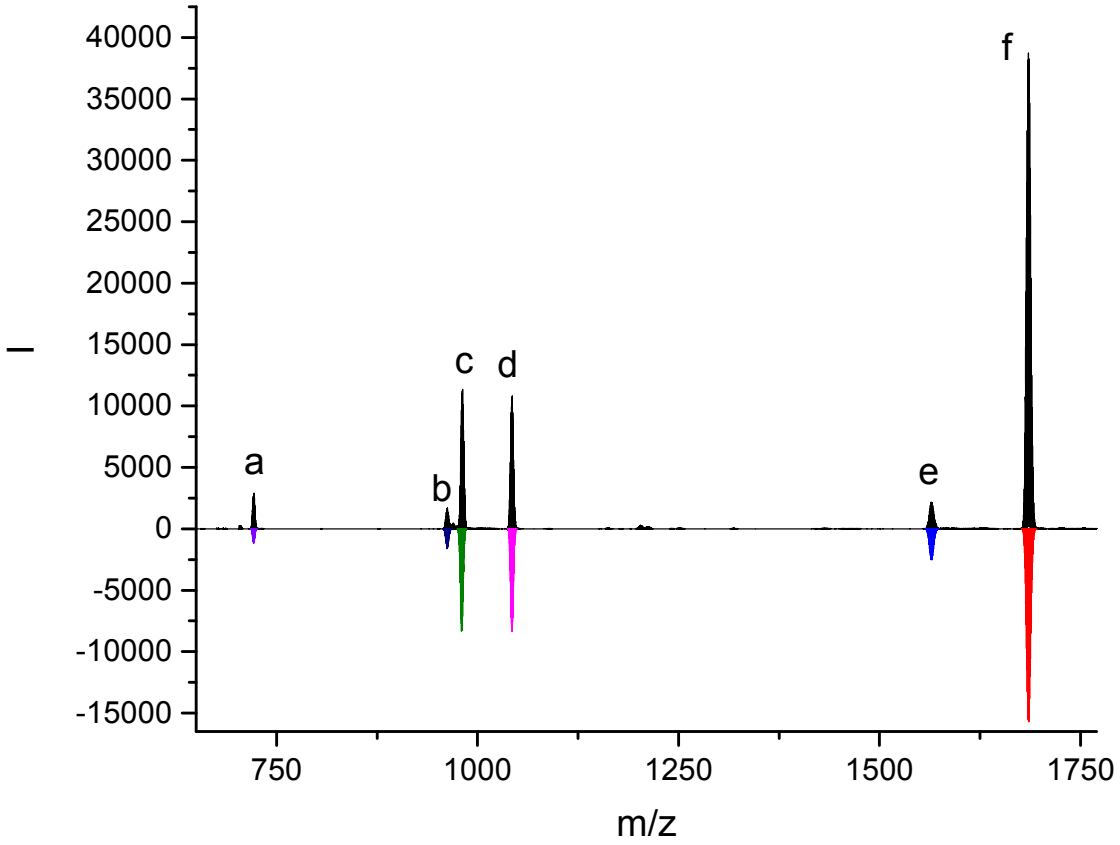

Table S2. Peak assignment for the spectrum of **1** presented in Fig. S1.

peak	anion	m/z exp	m/z calc
a	$[BiPW_{11}O_{39}]^{4-}$	721.550	721.548
b	$\{HBiPW_{11}O_{39}\}^{3-}$	962.398	962.400
c	$\{HBiPW_{11}O_{39}(H_2O)_3\}^{3-}$	980.400	980.415
d	$\{(Bu_4N)BiPW_{11}O_{39}\}^{3-}$	1042.883	1042.885
e	$\{(Bu_4N)HBiPW_{11}O_{39}\}^{2-}$	1564.830	1564.832
f	$\{(Bu_4N)_2BiPW_{11}O_{39}\}^{2-}$	1685.558	1685.560

Fig. S4. The comparison of observed and calculated isotopic patterns for the spectrum of **1** presented in Fig. S1.

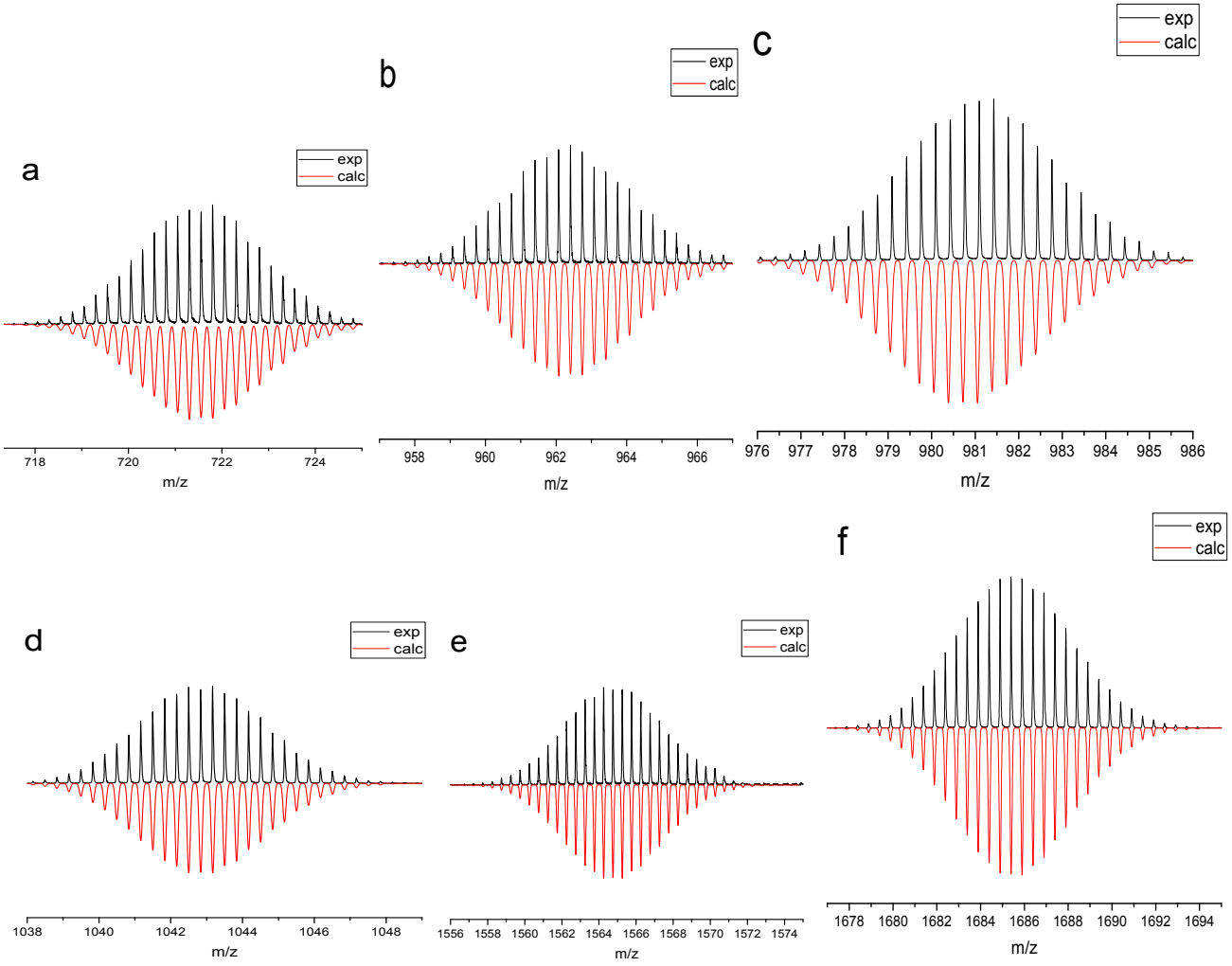

Fig. S5. Full HR-ESI-MS(-) spectrum for **2** in CH_3CN.

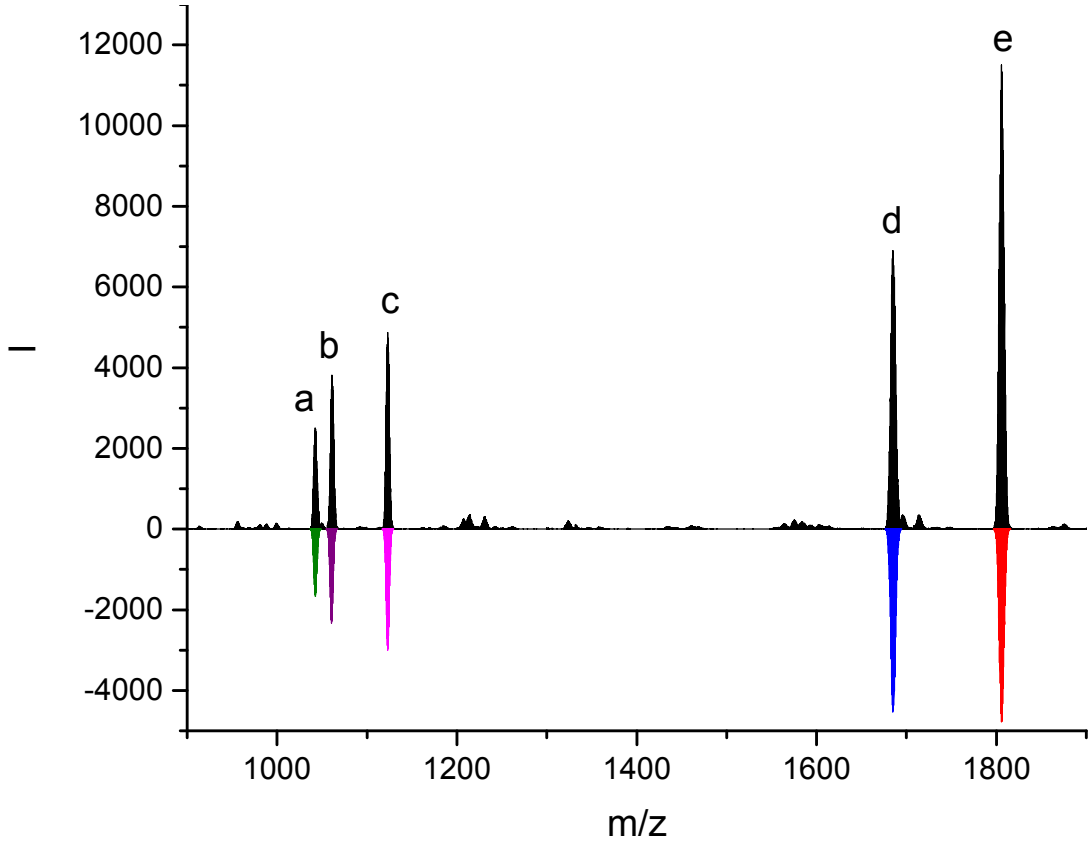

Table S3. Peak assignment for the spectrum of **2** presented in Fig. S3.

peak	anion	m/z exp	m/z calc
a	$\{(Bu_4N)HPbPW_{11}O_{39}\}^{3-}$	1042.630	1042.634
b	$\{(Bu_4N)HPbPW_{11}O_{39}(H_2O)_3\}^{3-}$	1060.659	1060.649
c	$\{(Bu_4N)_2PbPW_{11}O_{39}\}^{3-}$	1123.118	1123.119
d	$\{(Bu_4N)_2HPbPW_{11}O_{39}\}^{2-}$	1685.179	1685.182
e	$\{(Bu_4N)_3PbPW_{11}O_{39}\}^{2-}$	1805.911	1805.910

Fig. S6. The comparison of observed and calculated isotopic patterns for the spectrum of **2** presented in Fig. S3.

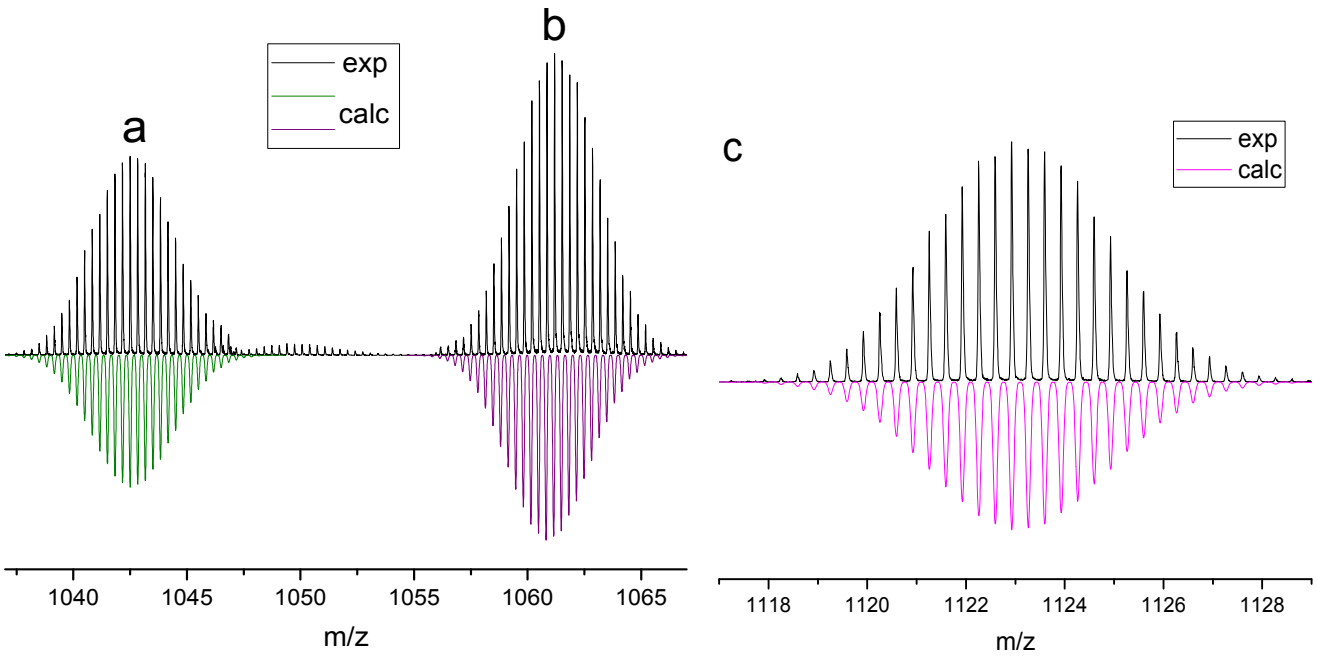

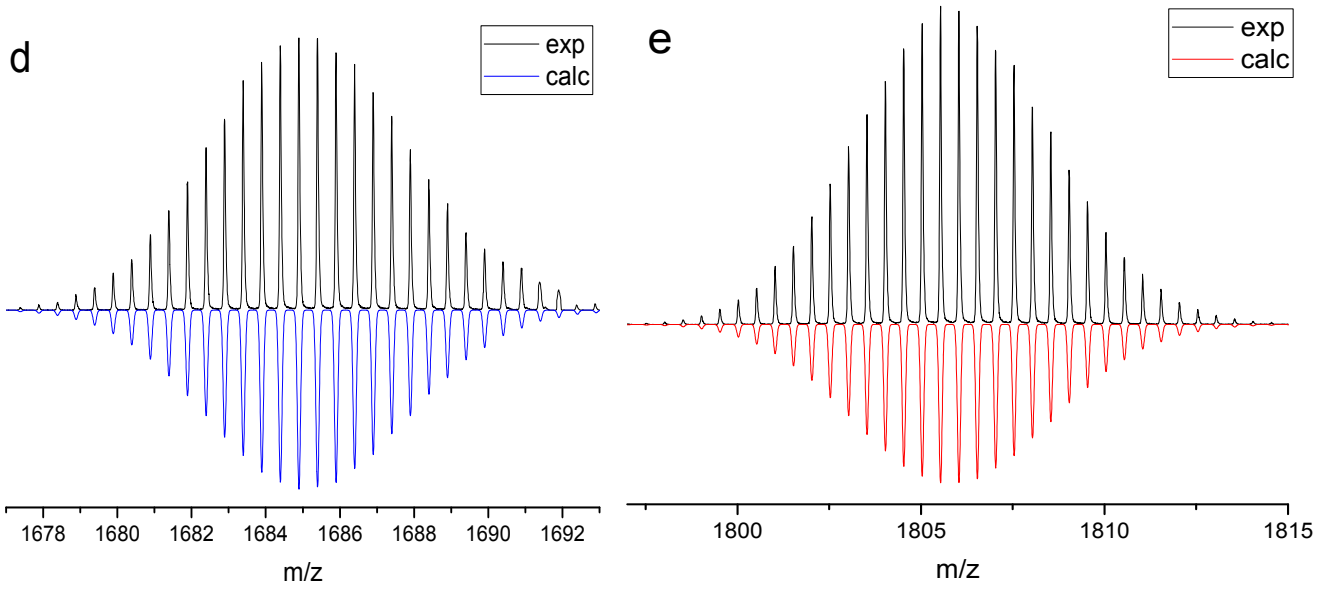
d
exp
calc
1678
1680
1682
1684
1686
1688
1690
1692
m/z
e
exp
calc
1800
1805
1810
1815
m/z

CV data

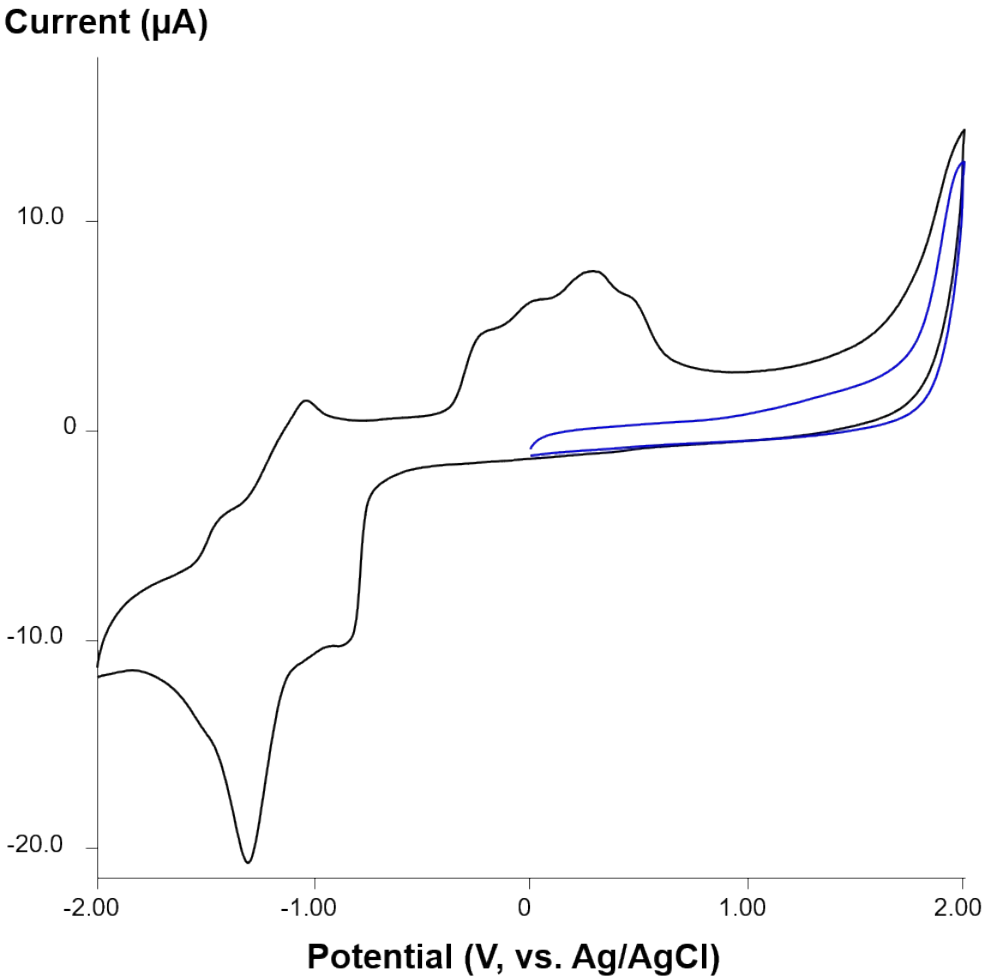

Fig. S7. CV of **1** in CH_3CN in the range from -2 to 2 V (black line) and from 0 to 2 V (blue line) at potential scan rate of 100 mV/s.

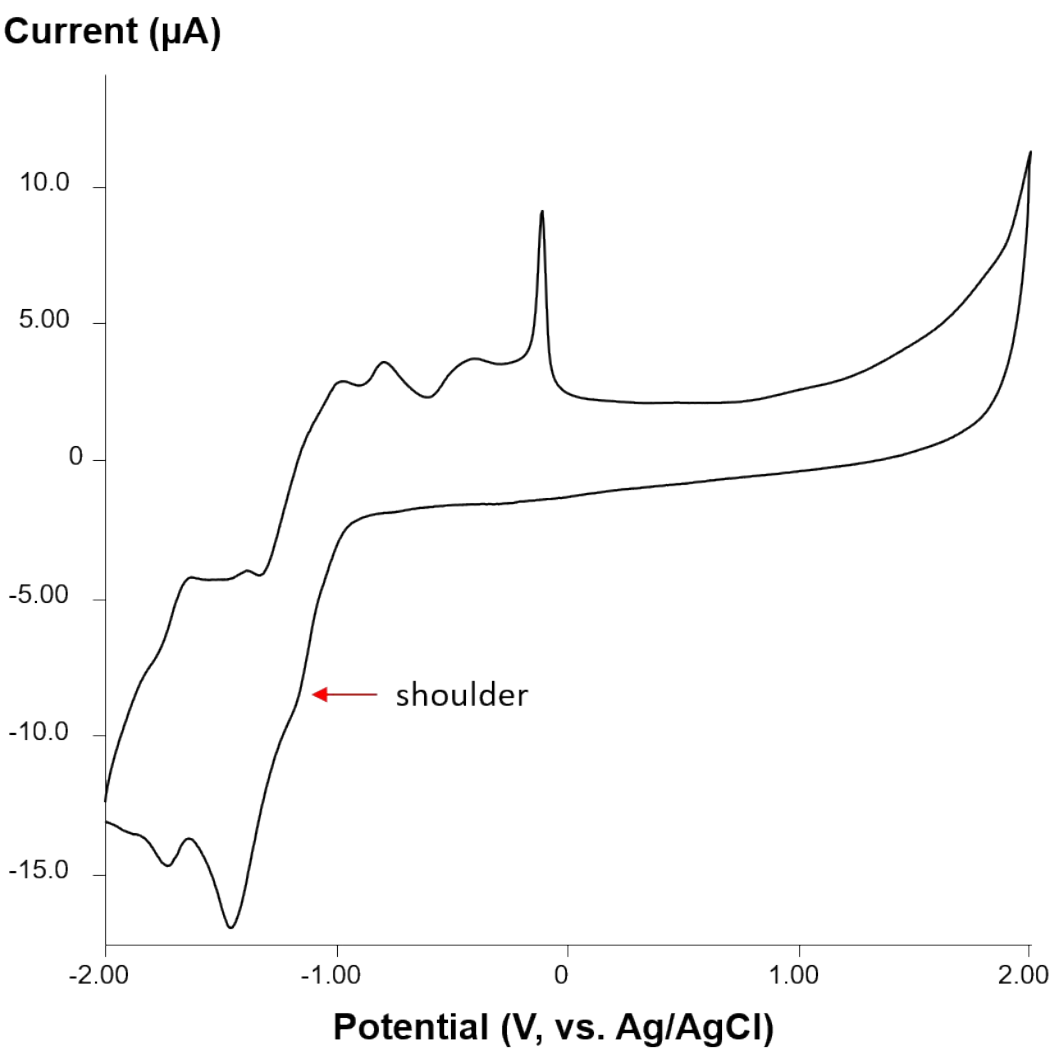

Fig. S8. CV of **2** in CH_3CN in the range from -2 to 2 V at potential scan rate of 100 mV/s.

Table S4. Redox potentials[a] for **1** and **2** in CH_3CN.

Cathodic potential	**1**	**2**
$E_c(1)$	-	-
$E_c(2)$	-0.82	-1.16 (shoulder)
$E_c(3)$	-1.27	-1.51
$E_c(4)$	weak peak	-1.76

[a] *E*, V versus Ag/AgCl; the potentials were measured at 100 mVs^{-1}; ferrocene was used as an internal standard, the Fc/Fc+ potential was 0.43 V

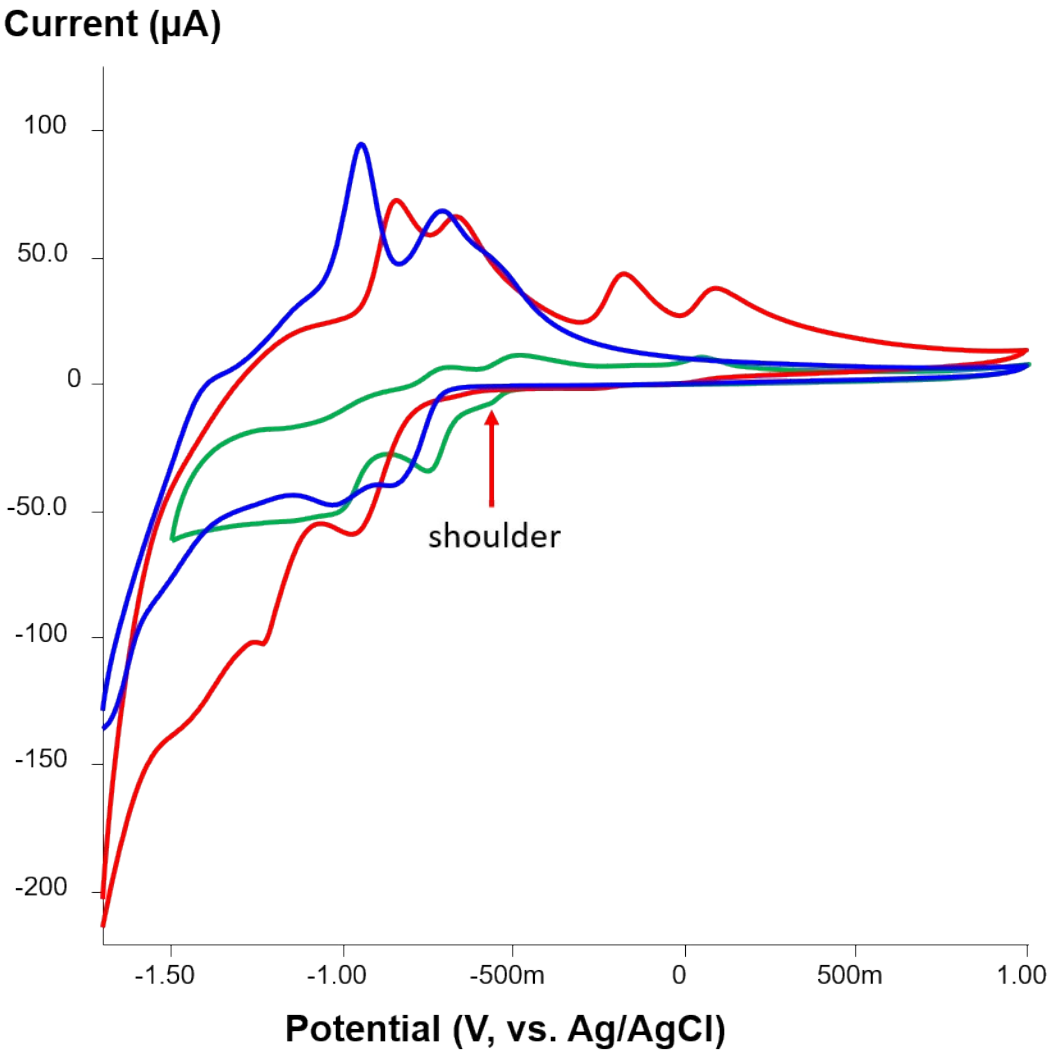

Fig. S9. CVs of **PW11O39** (red line) and **PW11O39/Y** (blue line) in H_2O with 1 M KCl as supporting electrolyte in the range from -1.7 to 1 V at potential scan rate of 100 mV/s. CV of **3** (green line) in H_2O with 1 M Li_2SO_4 as supporting electrolyte at pH = 4 in the range from -1.5 to 1 V at potential scan rate of 100 mV/s.

Quantum-chemical calculations

Table S5. The average distances in $[PW_{11}O_{39}X]^{n-}$ (X=Bi, BiO, n=4; X=Pb, PbO, n=5) complexes.

	P-O	W-O	M-O	W-$_{\mu 2}$O	M-$_{\mu 2}$O	M-O$_P$
$[PW_{11}O_{39}Bi]^{4-}$	1.56	1.73	n/a	1.93	2.24	2.54
$[PW_{11}O_{39}BiO]^{4-}$	1.56	1.73	1.98	1.93	2.19	2.70
$[PW_{11}O_{39}Bi]^{6-}$	1.56	1.75	n/a	1.94	2.42	3.00
$[PW_{11}O_{39}Pb]^{5-}$	1.56	1.74	n/a	1.93	2.36	2.84
$[PW_{11}O_{39}PbO]^{5-}$	1.56	1.74	2.01	1.93	2.28	2.93

Table S6. The average charges in $[PW_{11}O_{39}X]^{n-}$ (X=Bi, BiO, n=4; X=Pb, PbO, n=5) complexes.

	P	O$_{(-P)}$	W	M	O$_{(-W)}$	O$_{(-M)}$	$_{mu2}$O
$[PW_{11}O_{39}Bi]^{4-}$	3.54	-1.45	2.92	1.83	-0.88	n/a	-1.08
$[PW_{11}O_{39}BiO]^{4-}$	3.56	-1.45	2.92	2.35	-0.87	-0.92	-1.07
$[PW_{11}O_{39}Bi]^{6-}$	3.54	-1.45	2.91	0.75	-0.96	n/a	-1.08
$[PW_{11}O_{39}Pb]^{5-}$	3.55	-1.45	2.92	1.30	-0.93	n/a	-1.08
$[PW_{11}O_{39}PbO]^{5-}$	3.54	-1.45	2.92	1.93	-0.91	-0.97	-1.07

Table S7. The average parameters of *bcp* points in $[PW_{11}O_{39}X]^{n-}$ (X=Bi, BiO, n=4; X=Pb, PbO, n=5) complexes. Electron density (ρ), laplacian of electron density ($\nabla^2\rho$) and total energy density (H=V+G) values are in a.u. The ratio of absolute value of potential energy density to kinetic energy density (|V|/G) is dimensionless value.

$[PW_{11}O_{39}Bi]^{4-}$

bond	ρ	$\nabla^2\rho$	|V|/G	H
W-O$_{term}$	0.245	0.897	1.389	-0.143
W-$_{\mu 2}$O	0.144	0.582	1.239	-0.046
W-O(P)	0.037	0.140	1.020	-0.001
Bi-$_{\mu 2}$O	0.075	0.258	1.170	-0.013
Bi-O(P)	0.038	0.121	1.036	-0.001
P-O	0.203	0.674	1.501	-0.169

$[PW_{11}O_{39}BiO]^{4-}$

bond	ρ	$\nabla^2\rho$	|V|/G	H
W-O$_{term}$	0.246	0.904	1.390	-0.145
W-$_{\mu 2}$O	0.143	0.581	1.239	-0.046
W-O(P)	0.038	0.148	1.026	-0.001
Bi-O$_{term}$	0.131	0.423	1.306	-0.047

Bi-$_{\mu2}$O	0.083	0.272	1.198	-0.017
Bi-O(P)	0.028	0.088	0.966	0.001
P-O	0.203	0.685	1.497	-0.169

$[PW_{11}O_{39}Pb]^{5-}$

bond	ρ	$\nabla^2\rho$	|V|/G	H
W-O_{term}	0.238	0.878	1.381	-0.135
W-$_{\mu2}$O	0.144	0.581	1.241	-0.047
W-O(P)	0.037	0.141	1.023	-0.001
Pb-$_{\mu2}$O	0.056	0.205	1.086	-0.005
Pb-O(P)	0.019	0.067	0.887	0.002
P-O	0.202	0.660	1.505	-0.168

$[PW_{11}O_{39}PbO]^{5-}$

bond	ρ	$\nabla^2\rho$	|V|/G	H
W-O_{term}	0.240	0.885	1.383	-0.137
W-$_{\mu2}$O	0.144	0.581	1.240	-0.047
W-O(P)	0.039	0.148	1.027	-0.001
Pb-O_{term}	0.120	0.405	1.266	-0.037
Pb-$_{\mu2}$O	0.067	0.243	1.121	-0.008
Pb-O(P)	0.016	0.056	0.859	0.002
P-O	0.203	0.673	1.501	-0.169

Table S8. The calculated shielding constants (σ_{calc}), shielding constants averaged between symmetry equivalent atoms (σ_{avg}), chemical shifts calculated from fitted equation (δ_{calc}) and experimental chemical shift values (δ_{exp}) for $[PW_{11}O_{39}Bi]^{4-}$.

	σ_{calc}, ppm	σ_{avg}, ppm	δ_{calc}, ppm	δ_{exp}, ppm
W1	3308.50; 3307.49	3308.00	-119.01	-122.27
W2	3305.05; 3304.63	3304.84	-116.31	-118.73
W3	3288.87; 3287.63	3288.25	-102.09	-97.63
W4	3282.06	3282.06	-96.78	-94.86
W5	3279.83; 3279.09	3279.46	-94.56	-91.16
W6	3228.96; 3228.69	3228.83	-51.16	-53.44

Table S9. The calculated shielding constants (σ_{calc}), shielding constants averaged between symmetry equivalent positions (σ_{avg}), chemical shifts calculated from fitted equation (δ_{calc}) and experimental chemical shift values (δ_{exp}) for $[PW_{11}O_{39}Pb]^{5-}$.

	σ_{calc}	σ_{avg}	δ_{calc}	δ_{exp}
W1	3325.10; 3323.87	3324.49	-136.54	-133.63
W2	3301.20; 3300.42	3300.81	-113.93	-118.80
W4	3286.85	3286.85	-100.60	-101.61
W5	3277.19; 3276.41	3276.80	-91.00	-96.39
W3	3271.21; 3269.99	3270.60	-85.08	-78.36
W6	3235.43; 3235.39	3235.41	-51.47	-51.90

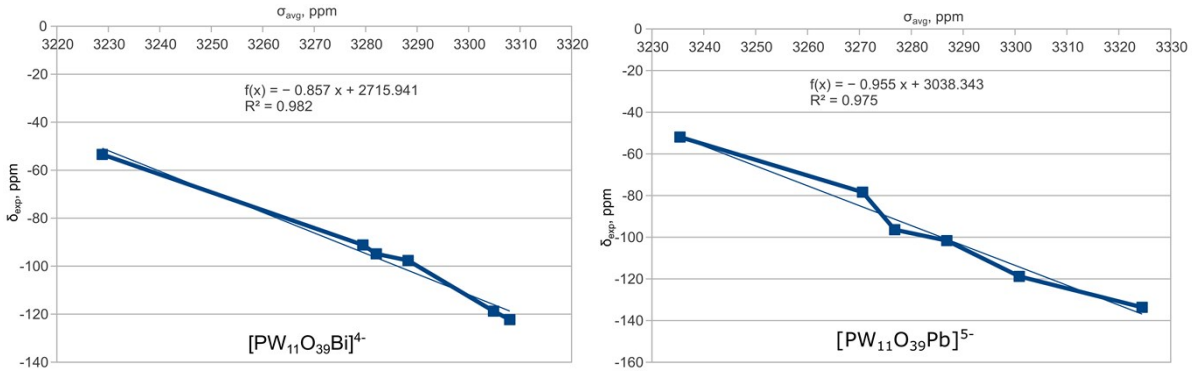

Fig. S10. Relation between average shielding constants (σ_{avg}) and experimental chemical shift (δ_{exp}) values for $[PW_{11}O_{39}Bi]^{4-}$ (left) and $[PW_{11}O_{39}Pb]^{5-}$ (right).

Table S10. Local atomic structure parameters: N – coordination number, R – interatomic distance, σ^2 – Debye–Waller factor, and F – quality of the fitting.

	R, Å	σ^2, Å^2	N	F-factor, %
2				
Pb-O	2.28(2)	0.0076(7)	4	1.1
Pb-W	3.66(9)	0.009(2)	3	
PbO				
Pb-O	2.29(2)	0.0084(8)	4	2.7
Pb-Pb	3.68(5)	0.006(1)	4	
Pb-Pb	3.83(6)	0.011(4)	4	
Pb-Pb	3.96(6)	0.011(4)	4	

PL data

Luminescence

Corrected luminescence spectra were recorded on a Fluorolog 3 spectrometers (Horiba Jobin Yvon) with a R928 (FL-1073) photomultiplier and two Czerny–Turner double monochromators. Temperature dependences of luminescence were studied out using Optistat DN optical cryostat (Oxford Instruments).

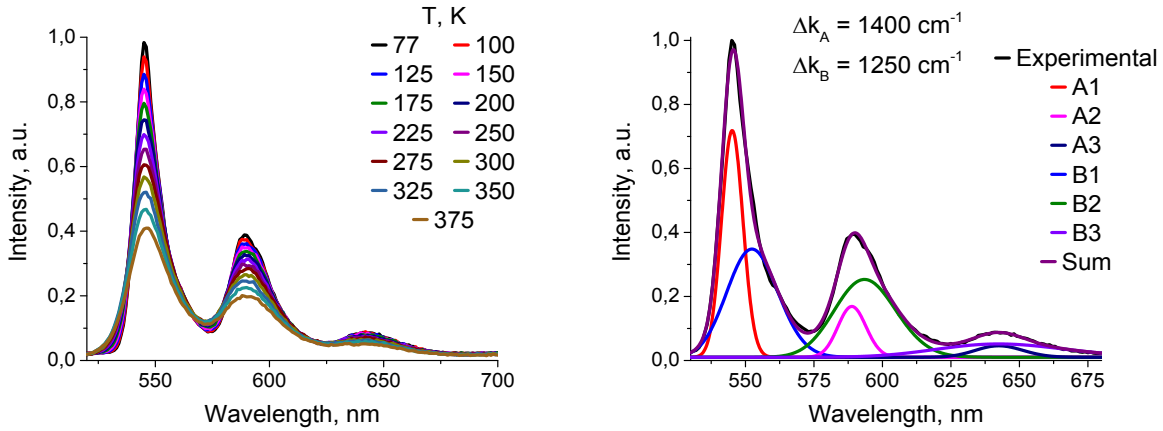

Fig. S11. Temperature dependence of the PL (λ_{Ex} = 500 nm) (left) and the Gaussian fits of PL spectrum (right) recorded at 77 K.

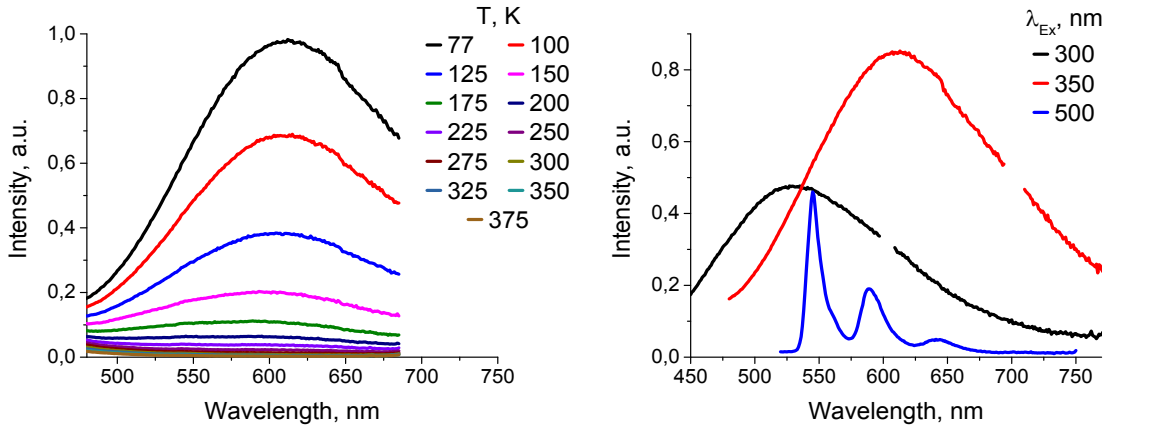

Fig. S12. Temperature dependence of the PL (λ_{Ex} = 350 nm) spectra of **1** and excitation dependence of the PL spectra at 77 K.

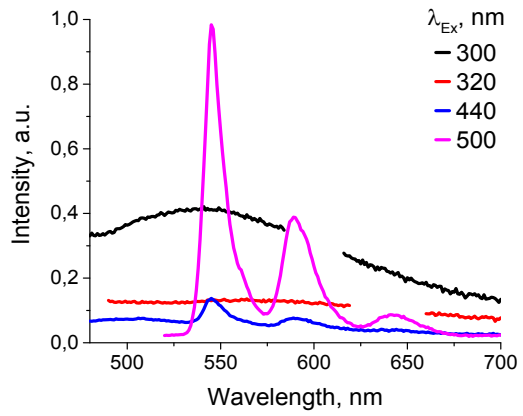

Fig. S13. Excitation dependence of the PL spectra of **2**(wet) at 77 K.

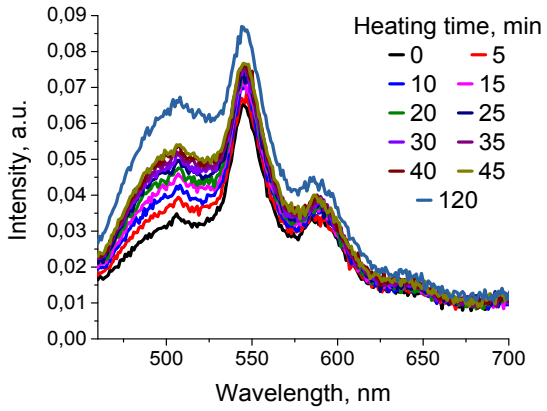

Fig. S14. The time-dependence of the PL (λ_{Ex} = 440 nm) spectrum of **2**(wet) at 50°C

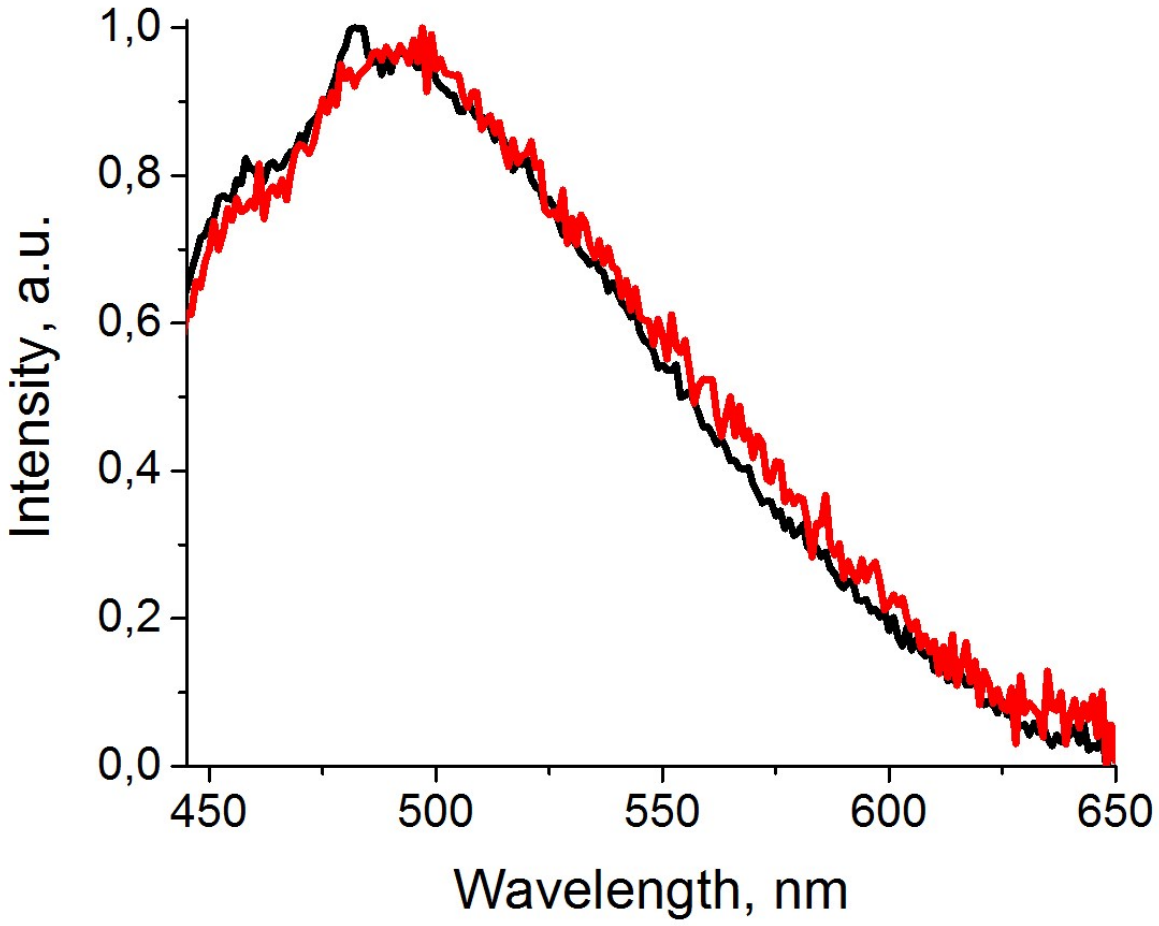

Fig. S15. PL (λ_{Ex} = 420 nm) spectra of dry (black) and wet (red) complex **3**.

XRD data

X-ray crystallography.

The crystal data and refinement details for the crystal structure of **3** are summarized in Table S11. The diffraction data were collected on a Bruker D8 Venture diffractometer with a CMOS PHOTON III detector and IμS 3.0 source (Mo Kα radiation, λ = 0.71073 Å) at 150 K. The φ- and ω-scan techniques were employed. Absorption correction was applied by SADABS (Bruker Apex3 software suite: Apex3, SADABS-2016/2 and SAINT, version 2018.7-2; Bruker AXS Inc.: Madison, WI, 2017.). The structure was solved by SHELXT[23] and refined by full-matrix least-squares treatment against $|F|^2$ in anisotropic approximation with SHELX 2014/7[24] in ShelXle program.[25] H-atoms of TMA cations were refined in the geometrically calculated positions. The protons of water molecules of crystallization were not refined. The structural refinement of the current gives 6.17 K+ per formula, while ICP-AES of the isolated crystalline phase gives only 3 K+ per formula. This means presence of several types solid solutions with different K+/TMA+/H+ ratio. The main geometric parameters are summarized in Table S12.

The main structural building block is a sandwich-type $[(PW_{11}O_{39})_2Bi]^{11-}$ anion (Fig. S16), when Bi^{3+} has CN 8 with square-antiprismatic coordination arrangement. There are two independent $[(PW_{11}O_{39})_2Bi]^{11-}$ anions in the unit cell (in general and in special positions respectively). The Bi^{3+} arrangement in both type anions is shown in Fig. S17. Polyoxoanions form layered type packing with ABAB… motive (Fig. S18) in the crystal structure.

The crystallographic data have been deposed in the Cambridge Crystallographic Data Centre under the deposition codes CCDC 2055126.

XRPD

XRPD analysis of polycrystals was performed on Shimadzu XRD-7000 diffractometer (CoK-alpha radiation, Fe – filter, linear One Sight detector, 5 – 70° 2θ range, 0.0143° 2θ step, 2s per step).

References:

(23) Sheldrick, G. M. SHELXT – Integrated Space-Group and Crystal-Structure Determination. *Acta Crystallogr. Sect. A Found. Adv.* **2015**, *71* (1), 3–8.

(24) Sheldrick, G. M. Crystal Structure Refinement with SHELXL. *Acta Crystallogr. Sect. C Struct. Chem.* **2015**, *71* (1), 3–8.

(25) Hübschle, C. B.; Sheldrick, G. M.; Dittrich, B. ShelXle : A Qt Graphical User Interface for SHELXL. *J. Appl. Crystallogr.* **2011**, *44* (6), 1281–1284.

Table S11. Crystal data and structure refinement for **3**.

Identification code	**3**
Empirical formula	$C_{16}H_{61.5}BiK_{6.17}N_4O_{96.67}P_2W_{22}$
Formula weight	6413.49
Temperature/K	150(2)
Crystal system	monoclinic
Space group	*C*2/*c*
a/Å	48.525(3)
b/Å	12.6920(8)
c/Å	56.670(3)
α/°	90
β/°	109.593(2)
γ/°	90
Volume/Å^3	32881(3)
Z	12
ρ_{calc}g/cm^3	3.879
μ/mm^{-1}	24.953
F(000)	33642.0
Crystal size/mm^3	0.12 × 0.1 × 0.1
Radiation	MoKα (λ = 0.71073)
2Θ range for data collection/°	3.33 to 50.266
Index ranges	-57 ≤ h ≤ 57, -15 ≤ k ≤ 15, -67 ≤ l ≤ 67
Reflections collected	90876
Independent reflections	28621 [R_{int} = 0.0743, R_{sigma} = 0.0869]
Data/restraints/parameters	28621/390/1867
Goodness-of-fit on F^2	1.130
Final R indexes [I>=2σ (I)]	R_1 = 0.0722, wR_2 = 0.1298
Final R indexes [all data]	R_1 = 0.0994, wR_2 = 0.1391
Largest diff. peak/hole / e Å^{-3}	2.23/-2.12

Table S12. Selected bond lengths for **3**.

Atom	Atom	Length/Å	Atom	Atom	Length/Å
Bi1	O32	2.447(17)	W16	O59	1.88(2)
Bi1	O33	2.566(18)	W16	O60	1.68(2)
Bi1	O34	2.455(16)	W16	O61	1.90(2)
Bi1	O35	2.402(18)	W16	O73	2.42(2)
Bi1	O40	2.49(2)	W16	O76	1.90(2)
Bi1	O41	2.469(17)	W17	O40	1.78(2)
Bi1	O42	2.374(18)	W17	O43	1.66(3)
Bi1	O79	2.35(2)	W17	O45	2.03(2)
Bi2	O84	2.313(18)	W17	O46	2.358(19)
Bi2	O84[1]	2.313(18)	W17	O47	1.924(18)
Bi2	O85	2.388(17)	W17	O59	1.96(2)
Bi2	O85[1]	2.388(17)	W18	O41	1.791(15)
Bi2	O86[1]	2.614(17)	W18	O46	2.341(17)
Bi2	O86	2.614(18)	W18	O47	1.90(2)
Bi2	O87[1]	2.511(17)	W18	O48	1.707(19)
Bi2	O87	2.511(17)	W18	O49	1.929(18)
W1	O1	1.725(17)	W18	O54	2.065(19)
W1	O2	1.877(16)	W19	O57	1.877(19)
W1	O3	1.898(16)	W19	O58	1.92(2)
W1	O4	1.899(16)	W19	O73	2.451(18)
W1	O5	1.918(15)	W19	O77	2.00(2)
W1	O18	2.406(17)	W19	O78	1.740(19)
W2	O4	1.950(15)	W19	O79	1.76(2)
W2	O6	1.702(19)	W20	O49	1.888(19)
W2	O7	1.917(17)	W20	O50	1.894(16)
W2	O12	1.908(16)	W20	O51	1.716(18)
W2	O18	2.447(17)	W20	O52	1.87(2)
W2	O155	1.788(15)	W20	O53	2.403(16)
W3	O2	1.963(17)	W20	O64	1.927(17)
W3	O7	1.927(18)	W21	O42	1.749(18)
W3	O8	1.698(15)	W21	O50	1.940(16)
W3	O18	2.420(16)	W21	O53	2.446(17)
W3	O21	1.795(18)	W21	O55	2.028(17)
W3	O25	1.928(18)	W21	O56	1.65(2)
W4	O5	1.898(15)	W21	O57	1.942(18)
W4	O9	1.725(16)	W22	O67	1.917(19)
W4	O13	1.892(17)	W22	O69	1.69(2)
W4	O17	2.498(18)	W22	O71	1.87(3)
W4	O36	1.921(17)	W22	O72	1.91(2)
W4	O37	1.876(17)	W22	O74	2.40(2)
W5	O3	1.933(16)	W22	O75	1.95(2)
W5	O20	2.528(17)	W23	O101	1.92(2)
W5	O22	1.932(18)	W23	O102	1.69(2)

W5	O24	1.683(18)	W23	O103	1.876(19)
W5	O28	1.873(16)	W23	O105	1.909(19)
W5	O36	1.908(17)	W23	O106	1.910(17)
W6	O11	1.683(18)	W23	O114	2.407(16)
W6	O12	1.935(15)	W24	O98	1.896(18)
W6	O13	1.942(16)	W24	O103	1.97(2)
W6	O14	1.893(17)	W24	O114	2.429(15)
W6	O17	2.406(18)	W24	O143	1.689(17)
W6	O38	1.927(16)	W24	O144	1.845(19)
W7	O20	2.413(15)	W24	O145	1.891(19)
W7	O22	1.900(19)	W25	O96	1.846(16)
W7	O23	1.716(16)	W25	O97	2.515(17)
W7	O25	1.885(18)	W25	O99	1.930(16)
W7	O29	1.891(17)	W25	O100	1.941(18)
W7	O153	1.909(18)	W25	O101	1.93(2)
W8	O20	2.486(16)	W25	O120	1.681(19)
W8	O28	2.017(18)	W26	O100	1.891(18)
W8	O29	1.927(16)	W26	O106	1.914(17)
W8	O31	1.709(18)	W26	O107	1.703(18)
W8	O35	1.713(18)	W26	O109	1.971(17)
W8	O156	1.943(16)	W26	O113	2.497(16)
W9	O17	2.448(15)	W26	O118	1.853(16)
W9	O32	1.760(17)	W27	O90	1.826(17)
W9	O37	2.049(17)	W27	O105	1.976(18)
W9	O38	1.968(17)	W27	O108	1.894(18)
W9	O39	1.730(16)	W27	O110	1.673(19)
W9	O156	1.899(17)	W27	O114	2.457(16)
W10	O19	2.365(16)	W27	O145	1.957(19)
W10	O21	2.072(18)	W28	O89	1.925(16)
W10	O26	1.940(17)	W28	O91	1.877(16)
W10	O27	1.724(16)	W28	O108	1.924(18)
W10	O34	1.766(16)	W28	O109	1.896(16)
W10	O153	1.916(19)	W28	O111	1.726(18)
W11	O14	1.918(16)	W28	O113	2.409(15)
W11	O15	1.668(16)	W29	O93	1.853(16)
W11	O19	2.361(17)	W29	O94	1.929(17)
W11	O26	1.932(16)	W29	O97	2.421(16)
W11	O33	1.752(18)	W29	O98	1.913(18)
W11	O155	2.119(15)	W29	O99	1.915(18)
W12	O52	1.952(19)	W29	O117	1.733(17)
W12	O53	2.52(2)	W30	O84	1.748(18)
W12	O55	1.871(19)	W30	O92	1.922(15)
W12	O63	1.92(2)	W30	O94	1.936(17)
W12	O65	1.69(2)	W30	O96	2.039(15)
W12	O75	1.85(2)	W30	O97	2.434(18)

W13	O62	1.68(3)	W30	O125	1.692(18)
W13	O63	1.89(3)	W31	O87	1.755(18)
W13	O72	1.91(2)	W31	O88	1.945(16)
W13	O73	2.50(2)	W31	O93	1.952(16)
W13	O76	1.94(2)	W31	O112	2.372(16)
W13	O77	1.88(2)	W31	O115	1.702(17)
W14	O54	1.82(2)	W31	O144	2.060(18)
W14	O64	1.897(18)	W32	O85	1.786(17)
W14	O66	1.711(18)	W32	O89	1.946(15)
W14	O67	1.95(2)	W32	O92	1.919(15)
W14	O68	1.92(2)	W32	O113	2.418(17)
W14	O74	2.43(2)	W32	O116	1.707(18)
W15	O45	1.83(2)	W32	O118	2.056(17)
W15	O61	1.91(2)	W33	O86	1.740(18)
W15	O68	1.91(2)	W33	O88	1.925(16)
W15	O70	1.67(2)	W33	O90	2.070(18)
W15	O71	1.97(3)	W33	O91	1.927(16)
W15	O74	2.41(2)	W33	O112	2.340(17)
W16	O58	1.92(2)	W33	O129	1.721(16)

[1]1-X,+Y,3/2-Z

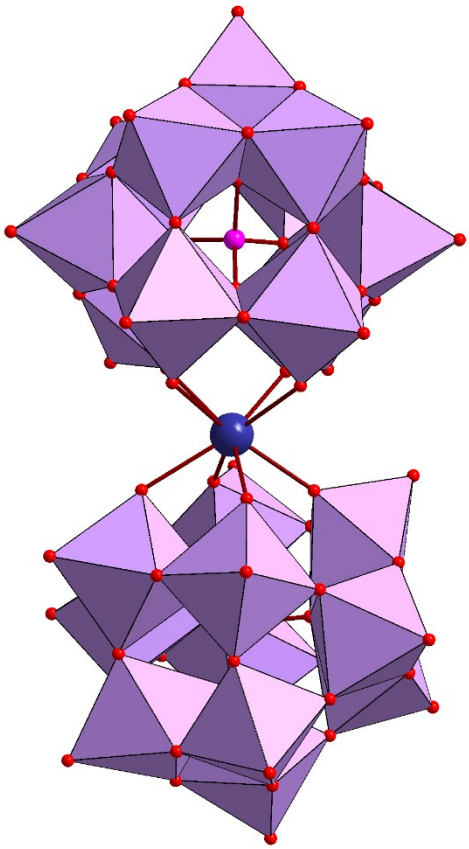

Fig. S16. The structure of polyoxometalate $[\{P_2W_{18}O_{39}\}_2Bi]^{11-}$ anion in **3**.

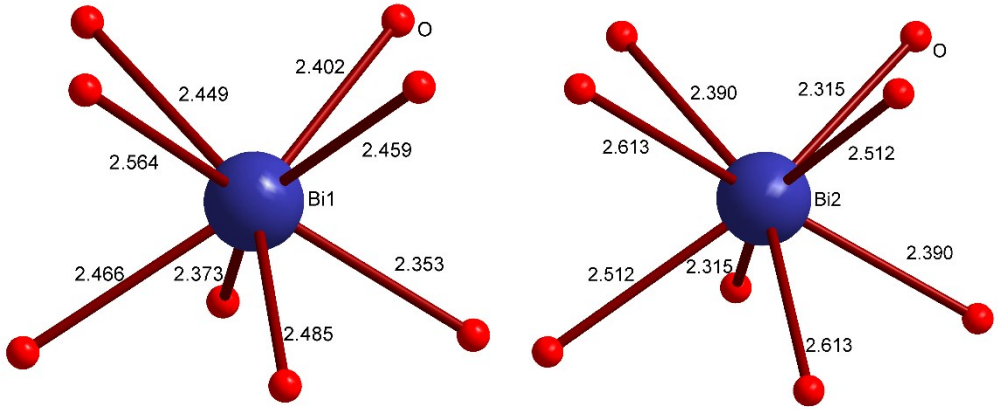

Fig. S17. Coordination polyhedron of two crystallographically independent Bi atoms in **3**, depicting Bi–O bond lengths.

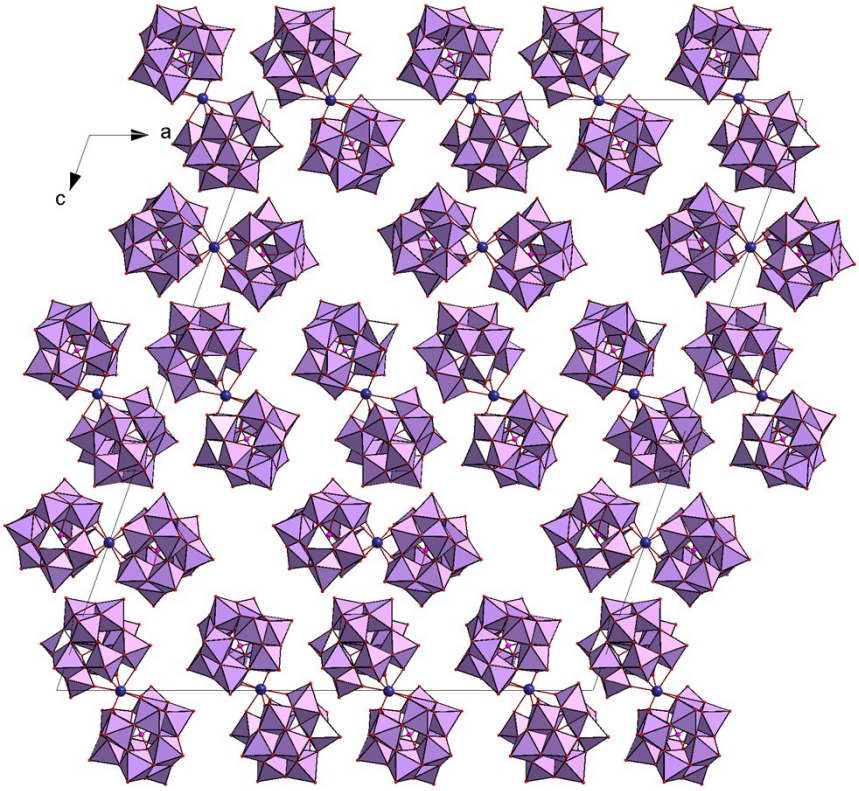

Fig. S18. Crystal packing of polyoxometalate $[\{P_2W_{18}O_{39}\}_2Bi]^{11-}$ anions in **3** along *b* axis. The cations and water molecules are not shown.